



AIAA 2002-4241

A Model of Hollow Cathode Plasma Chemistry

Ira Katz

John R. Anderson

James E. Polk

John R. Brophy

Jet Propulsion Laboratory
California Institute of Technology
Pasadena, CA

**38th AIAA/ASME/SAE/ASEE Joint Propulsion
Conference and Exhibit**

8-10 July 2002

Indianapolis, Indiana

For permission to copy or to republish, contact the copyright owner named on the first page.
For AIAA-held copyright, write to AIAA Permissions Department,
1801 Alexander Bell Drive, Suite 500, Reston, VA 20191-4344.

A Model of Hollow Cathode Plasma Chemistry

Ira Katz, John R. Anderson, James E. Polk, and John R. Brophy
MS 125-109
Jet Propulsion Laboratory
California Institute of Technology
4800 Oak Grove Dr
Pasadena, CA 91109
ira.katz@jpl.nasa.gov

Hollow cathodes with barium rich inserts are used in ion engines as electron sources both in the discharge chamber, and to neutralize the ion beam. Future ion engine missions will require hollow cathode lifetimes in excess of the 20,000 plus hours demonstrated during the Space Station hollow cathode life test. Depletion of free barium is one of the mechanisms that limit the life of hollow cathodes. We have developed a new model of hollow cathode plasma chemistry based on the observation that xenon ion mobility is diffusion limited due to resonant charge exchange reactions. The model shows that vapor phase barium atoms are ionized almost immediately and electric fields accelerate the ions upstream from the “emission zone”. We have also applied the model to the orifice region, where the resultant ion generation profile correlates with previously reported orifice erosion.

Introduction

Hollow cathodes are a critical component of most electrostatic and Hall effect ion thrusters. The record life of a hollow cathode was for the Space Station plasma contactor test run at NASA/GRC [1]. During this test, the hollow cathode performance changed after 23,000 hours of operation, and the cathode finally failed to restart after 28,000 hours, or just over 3 years. This endurance is impressive, and exceeds present demands on a hollow cathode for solar electric propulsion missions. However, on missions to the outer planets, electric thrusters will be required to operate for more than 5 years. Because of this need, we have

begun a systematic investigation to model the processes that can cause hollow cathode performance degradation and failure.

In a hollow cathode, electrons transfer between neutral gas atoms and ionized propellant through resonant charge exchange (CEX). The charge exchange cross-section between Xe and Xe⁺ is so large that inside hollow cathodes, ion mobility is diffusion limited. The model described below builds upon the limited ion mobility to construct a set of fluid equations that describe the cathode plasma chemistry. A straightforward application of the model leads to a new description of cathode processes.

In the orifice region, we have a new 1-D, variable cross section model that extends the previous model of Katz et. al. [2] to include charge exchange collisions, a radial density profile, axial variation in all parameters, and neutral gas viscosity. The model shows that the axial variation of ion currents bombarding the orifice walls is in agreement with published shapes of orifice erosion [3].

In the insert region, the electron temperature from this model agrees well with measurements by Malik, Montarde, and Haines [4]. The model shows that vapor phase barium atoms are quickly ionized, and the plasma electric fields rapidly transport barium ions upstream. This is in contrast with previous work [5] that only included neutral barium diffusion and convection downstream by neutral xenon gas. The effective velocities of barium ions are an order of magnitude greater and in the opposite direction than the barium neutral model reported previously.

Background

A hollow cathode consists of a metal tube lined with a barium oxide impregnated insert capped at one end by a plate with a small orifice as shown in Fig. 1. Propellant gas, typically xenon, flows into the tube and exits, partially ionized out the orifice. Electrons flow from the body of the cathode, through the orifice plasma to keeper and other anode surfaces. While most of the electrons emanate from the insert material, one of the new results in this paper is to show that an ampere or more of electrons are generated by ionization of the propellant gas, and the circuit completed by ions impacting the inner walls of the orifice.

The model presented below builds on a previously published model of orifice processes that ignored axial variation; instead it treated “the orifice as a cylinder containing a homogeneous neutral plasma” [2]. The previous zero-D model also assumed that the ion loss rate to the walls was the product of the wall area and the ion thermal flux, assuming the ions had a Maxwellian velocity distribution with the electron temperature. This simplifying assumption is removed in the present work, where the ion motion is determined from the ambipolar diffusion equation. Another approximation eliminated in the present model is the use of a temperature independent electron-neutral elastic cross section. The earlier model included power loss due to radiation; however, radiation is neglected in the present model because the xenon resonance lines are sufficiently narrow that most of the radiation is trapped inside the plasma [4].

Plasma Chemistry Model

Inside the orifice, the electron current density is the highest, and classical electron scattering leads to resistive heating. These hot electrons ionize a fraction of the Xenon gas, and, while most of the ions hit the walls of the orifice, some escape downstream. These ions provide charge neutralization for the electron current exterior to the cathode.

In the model, neutral xenon gas and electrons enter the orifice from the insert region, neutral xenon and electrons exit downstream, and xenon ions exit both upstream and downstream. The computational region includes the orifice and the chamfered expansion region,

shown in Fig. 2. Most of the ions that are created in the orifice recombine on the walls, as shown in Fig. 3. We assume that the electrons behave as a classical fluid, that the neutral Xenon gas flow is essentially collisionless, and that the ion flow is diffusion limited, because of the short mean free path, $< 10^{-5}$ m, for resonant charge exchange with neutrals. It is the very short ion mean free path for resonant charge exchange that controls the plasma density radial profile and loss rates.

Mass continuity equations

With the assumption of quasi neutrality $n = n_i \approx n_e$, the local ionization rate links the steady state continuity equations for all neutral xenon, xenon ions, and electrons.

$$-\dot{n} + \nabla \cdot u_0 n_0 = 0$$

$$\dot{n} + \nabla \cdot u_i n = 0 \quad ,$$

$$e\dot{n} + \nabla \cdot j_e = 0$$

where $j_e \equiv -enu_e$, and \dot{n} is the ion generation rate

$$\dot{n} = 4\sigma(T_e)n_0 n \sqrt{\frac{eT_e}{m_e}}$$

and $\sigma(T_e)$ is the impact ionization cross-section averaged over a Maxwellian distribution of electron energies,

$$\sigma(T_e) \approx [3.97 + (0.643T_e) - (0.0368T_e^2)] \text{Exp}\left(\frac{-12.127}{T_e}\right) 10^{-20}$$

Including the boundary condition that the ion flux to the orifice walls is balanced by the neutral flux off the walls, and integrating over the orifice radius, we obtain the following equations in the axial dimension, z.

$$\pi R^2 \left(-\dot{n} + \frac{\partial u_0 n_0}{\partial z} \right) + 2\pi R u_{wall} n = 0$$

$$\pi R^2 \left(\dot{n} + \frac{\partial u_i n}{\partial z} \right) - 2\pi R u_{wall} n = 0$$

$$\pi R^2 \left(e\dot{n} + \frac{\partial j_e}{\partial z} \right) = 0$$

where u_{wall} is the effective ion velocity to the walls, and $\pi R^2 j_e$ is the electron current, I_e . In the orifice, the u_{wall} is chosen to be the average radial velocity, u_r , derived later in this section. In the chamfered region, where the wall radius expands at a 45 angle the losses are lower, since the flow is nearly parallel to the walls. A true assessment of wall losses in the chamfered region requires a two-dimensional code. However, in the calculations below we have examined the effect of various choices for the wall loss velocity.

The electron continuity equation accounts for the increase in electron current due to ionization. This current is carried to the walls by the ions. Our calculations show that current from ionization can be nearly half the current for certain operating conditions.

The neutral gas velocity is determined assuming Poiseuille flow.

$$u_0 = -\frac{R^2 kT}{8\eta} \frac{dn}{dx}$$

The temperature dependent xenon viscosity is found using the corresponding states method [6]. For xenon the viscosity is

$$\eta = 2.3 \times 10^{-5} T_r^{0.71+0.29/T_r} \frac{Ns}{m^2} \text{ for } T_r \leq 1$$

$$T_r = \frac{T}{289.7}$$

The boundary condition for the upstream neutral density is that the sum of the neutral and ion fluxes leaving the orifice equal the specified gas flow rate into the hollow cathode.

Ion and electron momentum equations

We assume that inertial terms are negligible in both the ion and electron momentum equations, an assumption supported by the calculations below. We also assume that the ion current is small compared with the electron current. The electron momentum equation takes the familiar form of a generalized Ohm's law, as does the ion momentum equation.

$$n(u_i - u_0) = -D_i \frac{\partial n}{\partial z} + n \mu_i \mathbf{E}$$

$$j_e = e D_e \frac{\partial n}{\partial z} + e n \mu_e \mathbf{E}$$

where for each species the diffusion coefficient and the mobility are defined as

$$D_i = \tau_i \frac{kT_i}{M}, \quad D_e = \tau_e \frac{kT_e}{m_e}$$

$$\mu_i = \tau_i \frac{e}{M}, \quad \mu_e = \tau_e \frac{e}{m_e}$$

The ion momentum and electron momentum equations can be combined into a single equation

$$\begin{aligned} n(u_i - u_0) &= -\left(D_i + \frac{\mu_i}{\mu_e} D_e \right) \frac{\partial n}{\partial z} + \frac{\mu_i}{\mu_e} \left(\frac{j_e}{e} \right) \\ &= -D_\alpha \frac{\partial n}{\partial z} + \frac{\mu_i}{\mu_e} \left(\frac{j_e}{e} \right) \end{aligned}$$

where D_α is the ambipolar diffusion coefficient. Computational results show that the last term is non-negligible, and that the applied electric field drives ions in the orifice upstream into the insert

region. Therefore, ions generated in the insert region do not escape from the cathode.

The ion mobility is limited by resonant charge exchange with neutral Xenon. The cross section for Xenon ion – neutral charge exchange is 88 \AA^2 at 1 eV. In the orifice the ion mean free path for charge exchange collisions is only about ten microns. The ambipolar diffusion coefficient is

$$\begin{aligned} \tau_i &= \frac{1}{\sigma_{CEX} n_0 u_{scat}} \\ D_\alpha &= \frac{1}{\sigma_{CEX} n_0} \frac{e}{M} \left(\frac{T_i + T_e}{u_{scat}} \right) \end{aligned}$$

where u_{scat} is an effective ion speed including drift and thermal velocities. For relatively slow diffusion, such as in the insert region, u_{scat} can be approximated by the ion thermal speed, u_{th} . However, in the orifice the radial drift velocity frequently exceeds the ion thermal speed, and we use

$$\begin{aligned} u_{scat} &= \sqrt{u_{th}^2 + (u_i - u_0)^2 + u_r^2} \\ u_{th} &= \sqrt{\frac{eT_i}{M}} \end{aligned}$$

The collision time for electrons is given by

$$\tau_e = \frac{1}{\nu_{ei} + \nu_{en}}$$

where ν_{ei} is the electron-ion collision frequency and ν_{en} is the electron-neutral collision frequency. The electron-ion coulomb scattering from Reference [7] is

$$\nu_{ei} = 2.9 \times 10^{-12} n \Lambda T_e^{-3/2}$$

$$\Lambda = 23 - \frac{1}{2} L n \left(\frac{10^{-6} n}{T_e^3} \right)$$

and a numerical fit to the electron-neutral scattering cross section averaged over a Maxwellian electron distribution [8] (Mikelides, et. al., AIAA Paper 01-3355).

$$v_{en} = \sigma_{en}(T_e) n_0 \sqrt{\frac{eT_e}{m_e}}$$

$$\sigma_{en}(T_e) \approx 6.6 \times 10^{-19} \frac{\left(\frac{T_e}{4} - 0.1\right)}{\left[1 + \left(\frac{T_e}{4}\right)^{1.6}\right]}$$

Ion radial flow

Since axial ion density gradients in the interior of the orifice are small, most of the ions produced are lost by diffusion to the walls. Setting the diffusion loss rate equal to the ion production rate yields $-\nabla \cdot [D_a \nabla n] = \dot{n}$.

Ignoring the axial density gradients and radial variations in electron temperature and neutral densities, we obtain

$$\frac{\partial^2 n}{\partial r^2} + \frac{1}{r} \frac{\partial n}{\partial r} + C^2 n = 0$$

$$C^2 = \frac{n_0 \sigma(T_e) \sqrt{\frac{8eT_e}{\pi m_e}}}{D_a}$$

where $\sigma(T_e)$ is the electron impact ionization cross-section, averaged over a Maxwellian electron distribution. The solution to this equation is a zero order Bessel function

$$n(r) = n(0) J_0(Cr)$$

Assuming that the ion density goes to zero at the wall, the constant becomes

$$C = \frac{\lambda_{01}}{R}$$

where λ_{01} is the first zero of the zero order Bessel function. This eigenvalue

leads to the following equation that determines the electron temperature:

$$\left(\frac{R_0}{\lambda_{01}}\right)^2 n_0 \sigma(T_e) \sqrt{\frac{8eT_e}{\pi m_e}} - D_a = 0$$

The average ion density \bar{n} is related to the ion density on the centerline $n(0)$ by

$$\bar{n} = \frac{\int_0^R n(0) J_0\left(\frac{\lambda_{01}}{R_0} r\right) 2\pi r dr}{\pi R^2} = n(0) \left[\frac{2J_1(\lambda_{01})}{\lambda_{01}}\right]$$

In terms of the average ion density, the radial ion flux at the wall is

$$-D_a \frac{\partial n}{\partial r} = n(0) D_a \frac{\lambda_{01}}{R_0} J_1(\lambda_{01})$$

$$= \bar{n} D_a \frac{(\lambda_{01})^2}{2R_0} \equiv \bar{n} u_r$$

Substituting the ambipolar diffusion coefficient derived using the charge-exchange collision, the effective radial drift velocity at the wall is

$$u_r = \frac{(\lambda_{01})^2}{2R \sigma_{CEX} n_0} \frac{e}{M} \left(\frac{T_i + T_e}{u_{scat}}\right)$$

Energy equation

The steady-state electron energy equation is

$$0 = -\nabla \cdot \left(-\frac{5}{2} \mathbf{j}_e T_e - \kappa \nabla T_e\right) + \eta j_e^2 - \dot{n} E_i$$

where E_i is the ionization potential of Xenon, 12.1 eV. The plasma resistivity is

$$\eta = \frac{1}{\epsilon_0 \tau_e \omega_p^2}$$

and the classical electron thermal conductivity is [7]

$$\kappa = 3.2 \frac{\tau_e n e^2 T_e}{m_e}.$$

Following the analysis of Malik et. al.[4], it appears that the optical density at line centers is very thick, and therefore radiative losses are not included in most calculations. We have performed some calculations assuming that 10% of the radiation escaped, and with only minor differences to the results.

Insert Region Results

In the insert region, the electron current density is small, except in the vicinity of the orifice. If we drop the electron current terms and assume that the plasma is isothermal, we can use the ion radial flow equations to determine the maximum possible temperature. The model yields an electron temperature of 1.075eV compared with 1.1eV reported by Malik et. al.[4]. The difference is well within the uncertainty of either the model or the measurement.

We have solved in two dimensions the isothermal ambipolar diffusion equation to obtain a plasma density distribution inside the insert region. Fig. 4. The ion density in the orifice was fixed at 10^{22} m^{-3} , consistent with the results of the orifice calculations discussed in the next section. The plasma density drops rapidly upstream of the orifice. It can be shown analytically that if the radial variation were a zero order Bessel function, the plasma density would decay exponentially from the orifice.

Barium ions are accelerated upstream by the potentials in the insert region (Fig. 5). Since the barium ion charge exchange cross section with neutral xenon gas is not resonant, the scattering mean free path for barium ions with neutral xenon is an order of magnitude greater than that of xenon ions. As a result, the insert region electric fields drive the barium ions upstream with velocities of order several tens to a hundred meters per second. Thus the effective barium pressure above the active insert material is much lower than assumed in the previous work [5], and explains why the hollow cathode insert lifetimes are consistent with insert life in vacuum devices [9].

Orifice Results

We have applied the model to the NSTAR neutralizer cathode operating at the full power point [10]. At this operating point total cathode current is 3.26 A and the gas flow rate is 3.52 sccm.

Shown in Fig. 6 are the computed neutral xenon and ionized xenon number densities in the orifice and chamfer regions. The ion (plasma) density peaks near the center of the orifice and decreases on either side as ions flow out both ends of the orifice. The neutral xenon density decreases as the flow accelerates downstream. The computed upstream pressure for this case is 6.3 kPa (47 Torr). Computed pressures are typically within a factor of 2 of those measured experimentally.

The computed electron temperature, shown in Fig. 7, increases from 1.1 eV in the insert region to about 1.5 eV at the center of the orifice and then rises to

about 2 eV as the flow enters the chamfer region.

The calculated electron current through the orifice and chamfer regions is shown in Fig. 8. Most of the ions produced in the orifice diffuse to the wall, while the electrons produced from ionization collisions are extracted downstream. About 1 A of ion current strikes the orifice wall at NSTAR full power point. As a result only about 70% of the electrons extracted from the neutralizer cathode are supplied from the insert region.

Hollow cathode neutralizer orifice erosion has been reported in several long duration tests [1,3]. Typically the greatest enlargement is at the downstream side of the orifice, with the erosion diminishing toward the upstream end. For example, Fig. 9 shows a section through the NSTAR neutralizer hollow cathode orifice plate taken after the 8000 hr life test. The cylindrical orifice has been eroded into a conical shape, indicating an axial variation in the orifice environment. This same axial variation in erosion pattern was also reported in the life test of the International Space Station Plasma Contactor hollow cathode. In the present calculation, Fig. 10, the power going into ionization follows a similar profile. Almost all the ions generated are immediately accelerated radially into the orifice walls. We have not yet included double ions or sheath potentials into the model, and are therefore presently unable to calculate sputtering rates.

Summary and Conclusions

Taking advantage of the very short propellant ion mean free path for resonant charge exchange, we are developing a new model of hollow

cathode processes. Our first results, presented above paint a considerable different picture from previous models of how a hollow cathode works. The results include new descriptions of barium transport, current generation, operating pressure, and orifice erosion.

In the insert region, the model describes a weakly ionized, quasi-neutral plasma with relatively slow diffusion limited ion transport. Electron temperatures predicted by the model are in good agreement with recent data. Vapor phase barium atoms are immediately ionized due to their low, 5.2 eV, ionization potential. Previous models assumed barium transport was controlled by neutral gas convection. In our model, plasma electric fields drive barium ions upstream with velocities orders of magnitude greater and in the opposite direction from neutral gas convection.

When applied to the orifice, we found that a substantial fraction of the current was generated by ionization of the propellant, and subsequent recombination of the ions on the orifice walls. This process would allow a hollow cathode to continue to run even after the low work function material was depleted.

The ions charge exchange with neutrals many times as they are accelerated toward the orifice walls. These multiple charge exchange collisions act to heat the neutral gas far beyond the orifice plate temperature. This heating increases the gas viscosity, accounting for the pressure rise observed when a hollow cathode discharge is started.

The distribution and magnitude of ionization in the orifice correlates with

observed orifice erosion. Additional work in this area, including sheath potentials and double ion generation is needed to determine if ion bombardment is actually the source of orifice erosion.

Although the first results are promising, the work presented here is not a complete description of hollow cathode operation. We plan to develop a fully two-dimensional code that will include additional self-consistent models of insert electron emission, plasma sheaths, multiple ion species, and thermal conduction and radiation. The goal is the ability to reliably predict hollow cathode performance and life.

Acknowledgement

The research described in this publication was carried out at the Jet Propulsion Laboratory, California Institute of Technology.

References

- [1] Sarver-Verhey, T.R., "Destructive Evaluation of a Xenon Hollow Cathode After a 28,000 Hour Life Test," AIAA 98-3482, July 1998.
- [2] Katz, I., et al., "Model of Plasma Contactor Performance," Journal of Spacecraft and Rockets, v. 34, n. 6, p. 824-828, 1997.
- [3] Polk, J. E., et al., "An Overview of the Results from an 8200 Hour wear Test of the NSTAR Ion Thruster," AIAA 99-2446, June 1999.
- [4] Malik, A. K., et al., "Spectroscopic Measurements of Xenon Plasma in a Hollow Cathode," J. Phys. D: Appl. Phys. 33, p. 2307-2048, 2000.
- [5] Koveleski, S. D., "Life Model of Hollow Cathodes Using a Barium Calcium Aluminate Impregnated Tungsten Emitter," IEPC 01-276, October 2001.
- [6] Reid, R. C., et al, The Properties of Gases and Liquids, p. 403, McGraw-Hill, 1977.
- [7] Book, D. L., NRL Plasma Formulary, Naval Research Laboratory, 1987.
- [8] Mikelides, et. al., "A Hall Effect Thruster Plume Model Including Large-Angle Elastic Scattering," AIAA 01-3355, July 2001.
- [9] Palluel, P., et al., "Experimental Study of Impregnated-Cathode Behavior, Emission, and Life," J. Appl. Phys. 51(5), p. 2894-2902, May 1980.
- [10] Rawlin, V. K., "NSTAR Flight Thruster Qualification Testing," AIAA 98-3936, July 1998.

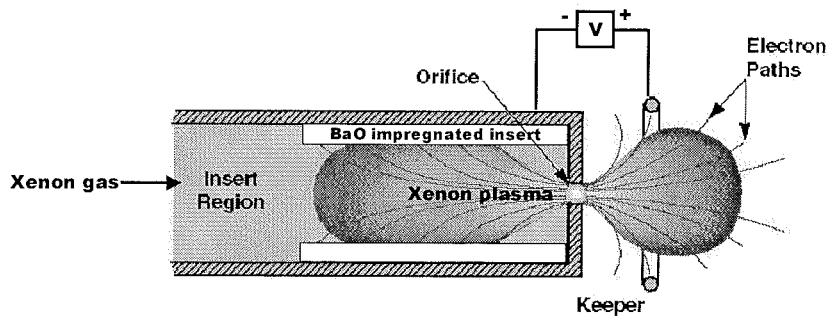


Fig. 1. Schematic of hollow cathode operation.

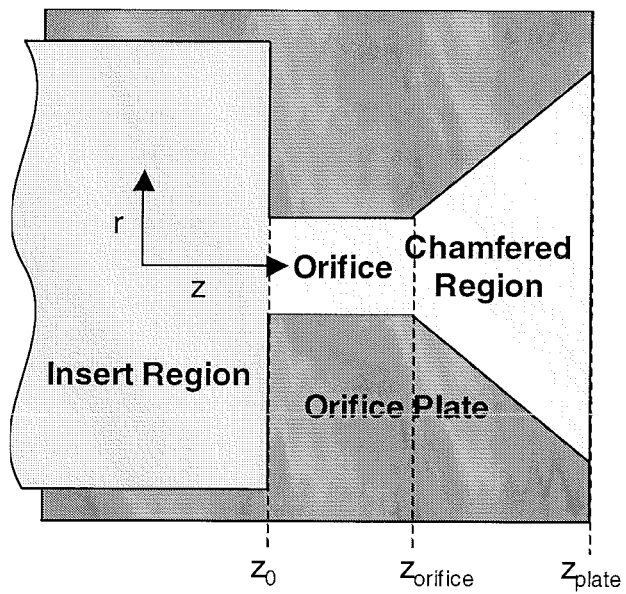


Fig. 2. The volume modeled includes the orifice and the chamfered region.

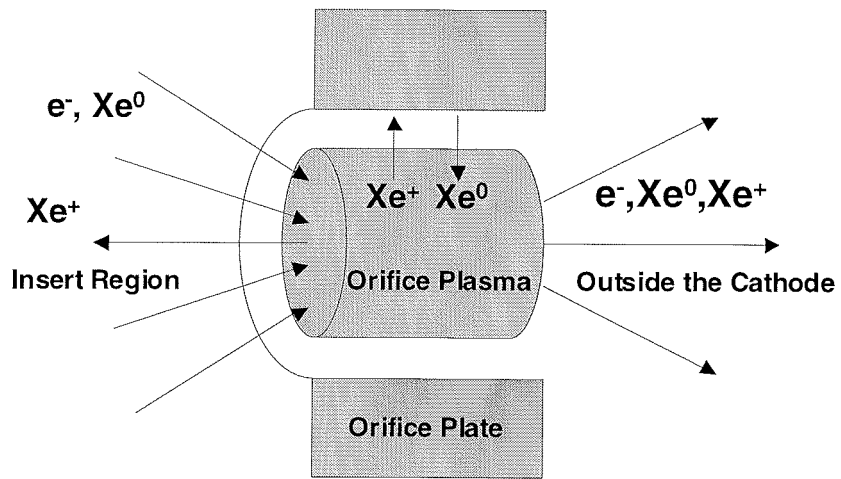


Fig. 3. Most of the ions created in the orifice recombine on the walls.

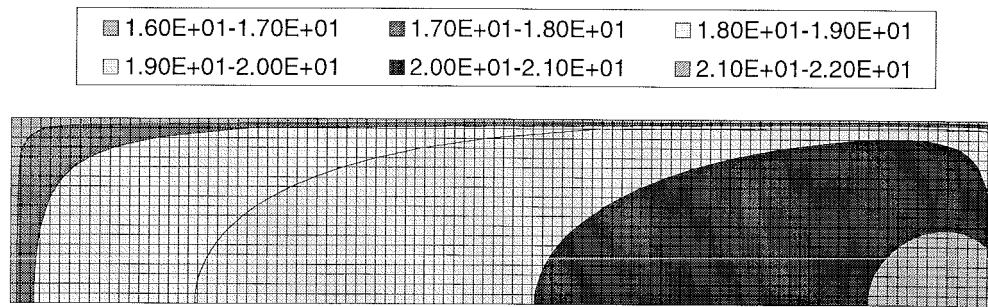


Fig. 4. Plasma density ($\log \# \text{ m}^{-3}$) in the insert region calculated assuming uniform electron temperature.

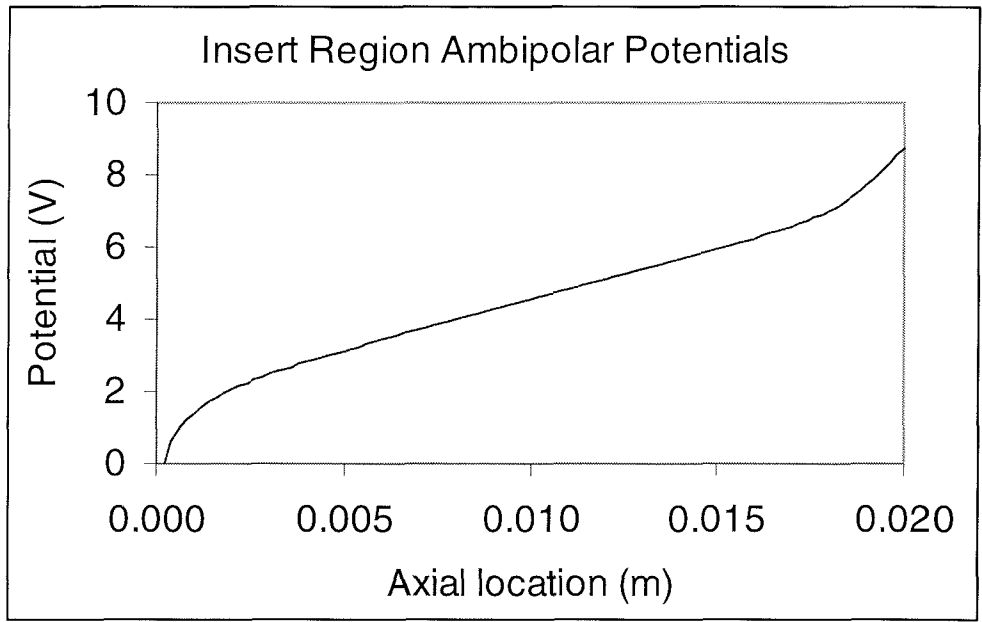


Fig. 5. Potential along the axis in the insert region.

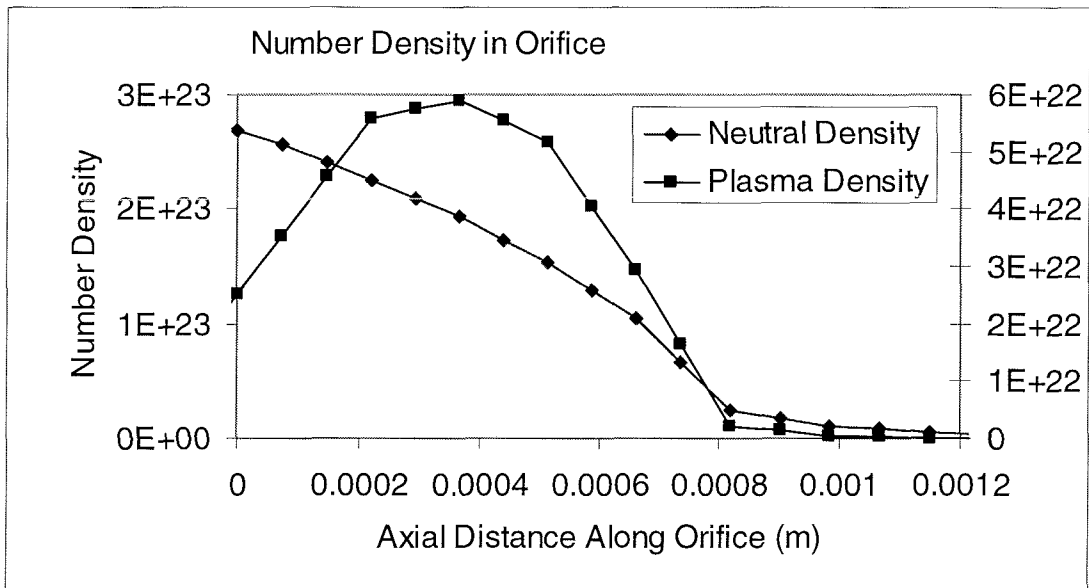


Fig. 6. Calculated neutral and ion densities in the orifice and expansion region

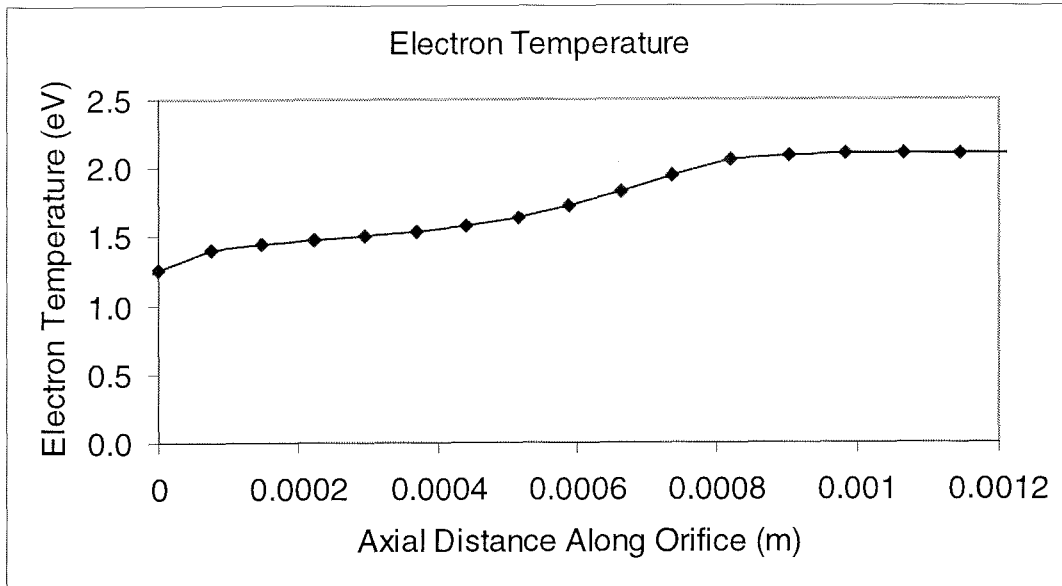


Fig. 7. Calculated electron temperatures in the orifice and expansion regions.

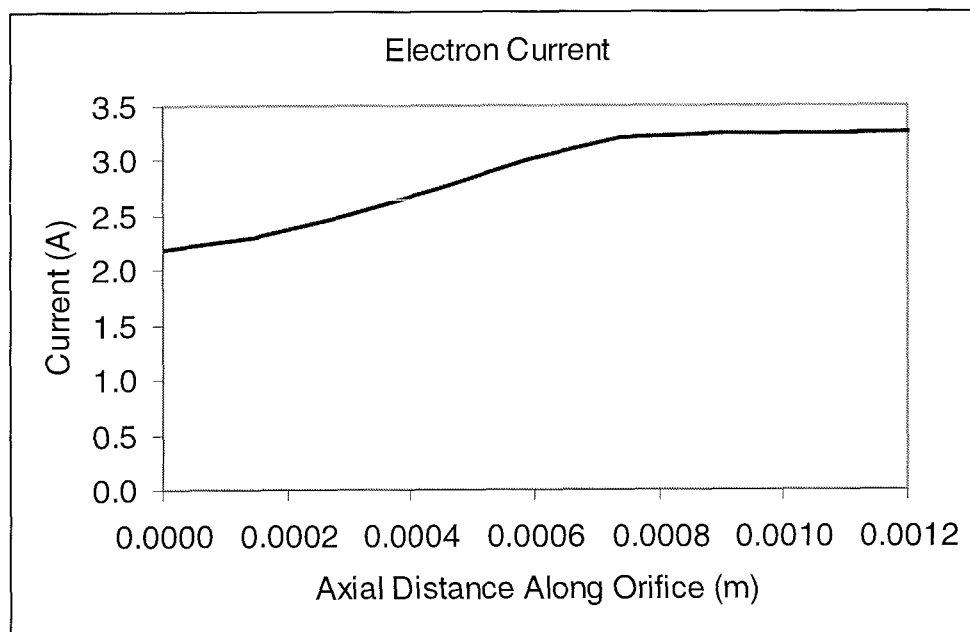


Fig. 8. Calculated electron current in the orifice and expansion regions.

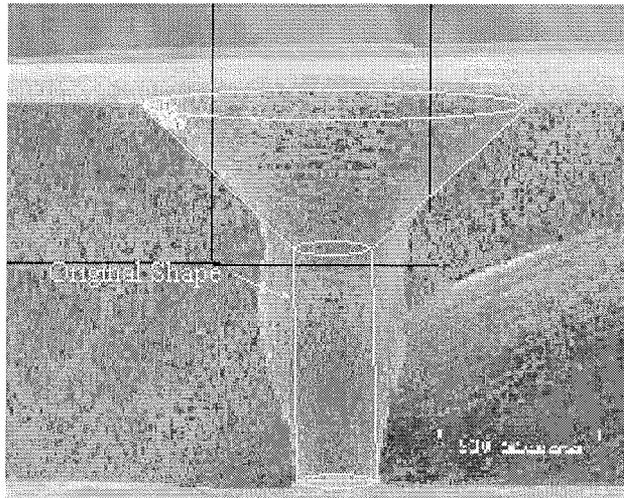


Fig. 9. Neutralizer cathode orifice showing erosion after long duration test [3]

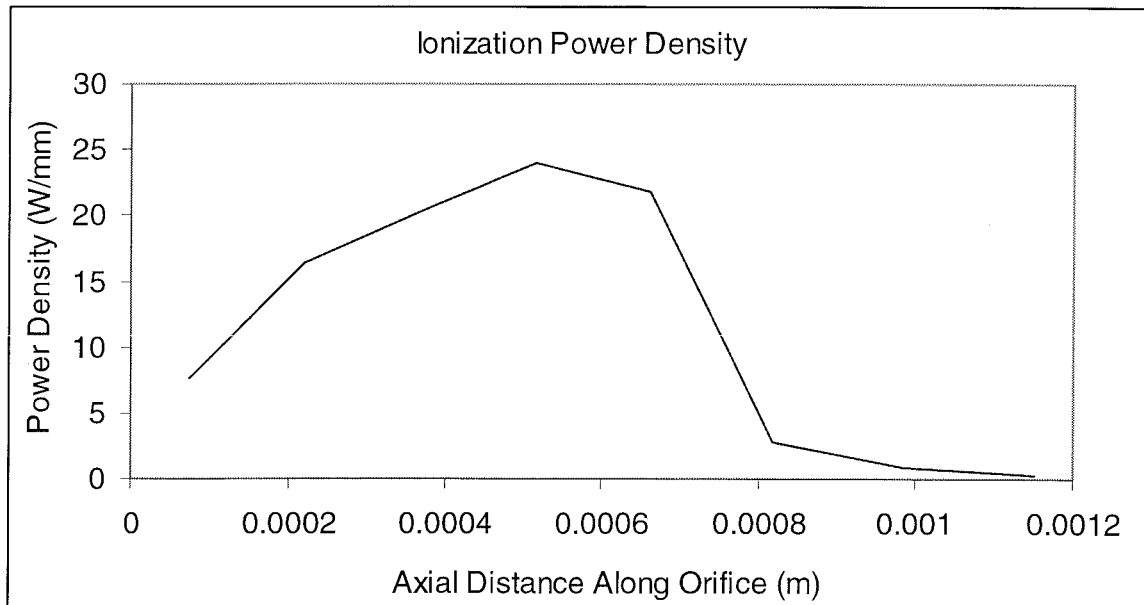


Fig. 10. Calculated ionization power density along the orifice.